View metadata, citation and similar papers at core.ac.uk

brought to you by CORE

provided by ScholarWorks@UNIST

AIP Physics of Plasmas

Electron bunching from a dc-biased, single-surface multipactor with realistically broad energy spectrum and emission angle of secondary electrons

Dongwon Shin, Seok-Gy Jeon, Jung-Il Kim, Geun-Ju Kim, and Min Sup Hur

Citation: Phys. Plasmas **19**, 023113 (2012); doi: 10.1063/1.3685697

View online: http://dx.doi.org/10.1063/1.3685697

View Table of Contents: http://pop.aip.org/resource/1/PHPAEN/v19/i2

Published by the AIP Publishing LLC.

Additional information on Phys. Plasmas

Journal Homepage: http://pop.aip.org/

Journal Information: http://pop.aip.org/about/about_the_journal

Top downloads: http://pop.aip.org/features/most_downloaded

Information for Authors: http://pop.aip.org/authors

ADVERTISEMENT

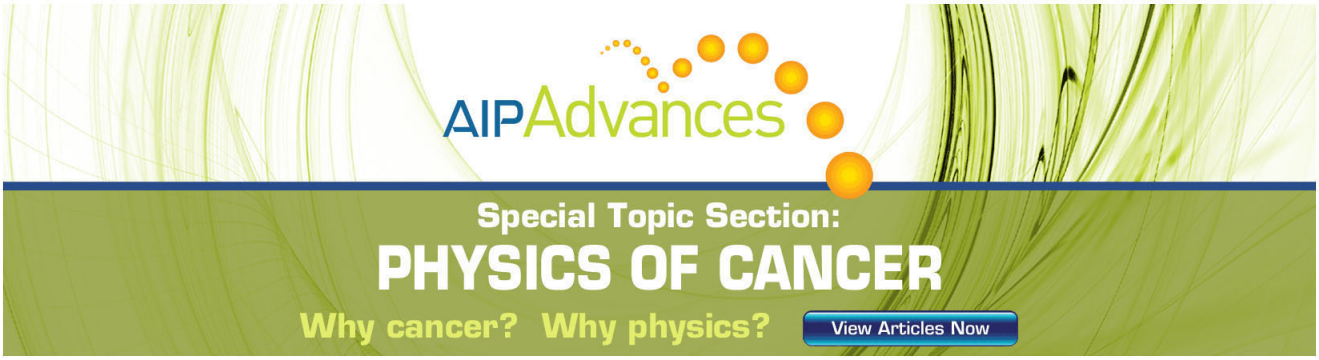

Downloaded 01 Aug 2013 to 114.70.7.203. This article is copyrighted as indicated in the abstract. Reuse of AIP content is subject to the terms at: http://pop.aip.org/about/rights_and_permissions

Electron bunching from a dc-biased, single-surface multipactor with realistically broad energy spectrum and emission angle of secondary electrons

Dongwon Shin,[1] Seok-Gy Jeon,[2] Jung-Il Kim,[2] Geun-Ju Kim,[2] and Min Sup Hur[1,a)]
[1]*UNIST, Banyeon-ri 100. Ulju-gun, Ulsan 689-798, South Korea*
[2]*Advanced Medical Device Research Center, KERI, 1271-19 Sa-dong, Ansan-si 426-170, South Korea*

(Received 25 October 2011; accepted 10 January 2012; published online 22 February 2012)

We studied the influences of wide energy spectrum and emission angle of secondary electrons on electron bunching from a dc-biased single surface multipactor. In our previous study of the same system, an ideally narrow energy spread of secondary electrons without emission angle was used in the analysis of the electron trajectory [M. S. Hur, J.-I. Kim, G.-J. Kim, and S.-G. Jeon, Phys. Plasmas **18**, 033103 (2011) and S.-G. Jeon, J.-I. Kim, S.-T. Han, S.-S. Jung, and J. U. Kim, Phys. Plasmas **16**, 073101 (2009)]. In this paper, we investigated the cases with realistic energy spectrum, which is featured by a wide energy spread and significant emission angle. To theoretically approach the matter of emission angle, we employed a concept of effective longitudinal velocity distribution. The theoretical results are verified by particle-in-cell (PIC) simulations. We also studied the electron bunching from a copper by PIC simulations, where we observed stable electron bunches with bunch width of approximately 80 μm. © *2012 American Institute of Physics*. [doi:10.1063/1.3685697]

I. INTRODUCTION

The multipactor discharge is prevalent in many rf devices.[3–8] Like other discharge processes, the multipactor is also associated with electron avalanche: some free initial electrons inside the device are accelerated by rf field to hit the material surface, yielding more secondary electrons. Then, the emitted secondary electrons hit again after several periods of the rf and make even more secondary electrons. As this procedure is periodically repeated, the number of free electrons in vacuum increases rapidly. This event, which occurs in most rf devices, is usually undesirable, since it can damage the window of the rf device[9–11] or change the conditions of device operation.[9] Sometimes the multipactor leads even to vacuum breakdown.[10,11]

Despite these undesirable features, there is a stream of utilizing it for a high intensity electron beam generation.[12,13] For example, there can appear electron bunches, which have narrow sizes and high intensities, if some inherent resonance conditions are satisfied.[1,2,13] The electron bunches generated in this way can be utilized as a source of an efficient and compact microwave generator. Due to the avalanche-like property of the multipactor, usually the current density is very high compared to the conventional device: we expect to obtain a bunch current of a few tens of mA or even A order from GHz resonators. Another major advantage is that the electron beams are generated in a "bunched" form, so there is no need to use a dc-ac beam converting system as in the conventional microwave generator such as klystron. Thus, the size of the conventional klystron can be reduced significantly keeping the high efficiency. The typical bunch size from the multipactor is a few pico-second in time domain (tens of microns in space domain), which is much shorter than the period of GHz driving, so it is advantageous to use high harmonics also. One of the multipactor discharge structures suitable for that purpose, i.e., the bunch generator, is the dc-biased single surface multipactor[2] (Fig. 1).

In our previous works on this system, the fixed point theory with space charge effect neglected has been studied.[1,2] From the theory and simulations, it was found that narrow bunches of electrons can be generated stably if some stability conditions are satisfied. Such conditions were derived analytically from the quadratic mapping of a given phase deviation to the next cycle phase deviation.[1,2] And from the same mapping, the effects of a small, square-shaped energy spread in the secondary emission energy have been investigated.[1]

In this paper, we extend our previous work to include more realistic effects. First of all, we investigated the cases with realistically wide spectrum of emission energy of the secondary electrons. The materials we first considered here are some artificial materials with broader spectra than before, and then we studied the case with a copper eventually. For analysis, we used the previously developed quadratic mapping[1] and particle-in-cell (PIC) simulations. Second, we considered the effects of emission angle of secondary electrons. For the implementation of the angle effect to our previous one-dimensional theory, we employed the concept of the "effective" secondary emission energy spectrum in normal direction to the surface. We compared the mapping theory with such "effective" spectrum with PIC simulations, from which a good agreement was obtained.

The paper is organized as follows: first, previous work on the fixed point theory is reviewed in Sec. II. Next, we present effective longitudinal energy spectrum by material property and angular effect of true secondary electron along with PIC simulation in Sec. III. Finally, we summarize in Sec. IV.

[a)]Electronic mail: mshur@unist.ac.kr.

 © 2012 American Institute of Physics

Downloaded 01 Aug 2013 to 114.70.7.203. This article is copyrighted as indicated in the abstract. Reuse of AIP content is subject to the terms at: http://pop.aip.org/about/rights_and_permissions

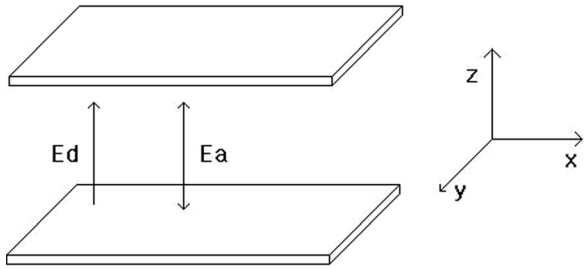

FIG. 1. The structure of the multipactor. Lower plates are surface which the electrons hit.

II. FIXED POINT THEORY

In this section, we review the fixed point equation to calculate analytically the electron trajectories for bunching and its stability condition. If the electron trajectory in the structure is assumed to depend only on the external dc and ac fields without space charge effect, the single electron equation of motion is given by

$$\frac{d^2z}{dt^2} = -\frac{e}{m}E_d - \frac{e}{m}E_a \sin(\omega t + \theta_0), \tag{1}$$

where E_d and E_a are amplitudes of dc and ac fields. E_d has to be large enough to yield secondary electrons. And also, E_a must be adequately larger than E_d to prevent premature impact. The integration of Eq. (1) yields the trajectory equation of the secondary electron,

$$z(t) = \left(v_0 - \frac{eE_a}{m\omega}\cos\theta_0\right)t - \frac{eE_d}{2m}t^2 + \frac{eE_a}{m\omega^2}[\sin(\omega t + \theta_0) - \sin\theta_0], \tag{2}$$

where $z(t=0) = 0$. When the electron returns to the emission plate after the nth cycle of ac field, the secondary electron should start with the same initial velocity v_0. So, with $z = 0$ at $t = 2\pi n/\omega$ in Eq. (2), the resonance equation is given by

$$\cos\theta_0 = \nu - n\pi\varepsilon, \tag{3}$$

where $\varepsilon = E_d/E_a$, $\nu = m\omega v_0/eE_a$. Here, ε represents the ratio of ac and dc fields and ν is the normalized emission velocity of secondary electrons.

For a resonant electron to tolerate any perturbed deviation from its resonant trajectory, it should be in a certain range of stability condition. To find the stability condition of the fixed point, we derived a quadratic function, which mapped the deviation $\Delta_k = \theta_k - \theta_0$ at the kth cycle to Δ_{k+1} at the next cycle. If it takes τ_k for an electron to finish its cycle, $\Delta_{k+1} = \theta_{k+1} - \theta_0 = \theta_k + \tau(\theta_k) - \theta_0 - \tau(\theta_0)$, where $\tau(\theta_0) = 2n\pi$ and τ is the time for the electron to return to the emission plate. Here, θ_k is the initial phase at the kth cycle, and θ_0 is the fixed point from Eq. (2). By Taylor expansion up to the second order of Δ_k, we obtain

$$\frac{\Delta_{k+1}}{\Delta_k} = 1 + \frac{\tau(\theta_k) - \tau(\theta_0)}{\theta_k - \theta_0} \approx 1 + \left.\frac{\partial\tau}{\partial\theta}\right|_{\theta_0} + \frac{\Delta_k}{2}\left.\frac{\partial^2\tau}{\partial\theta^2}\right|_{\theta_0}. \tag{4}$$

From $z(\tau/\omega) = 0$, we could obtain $\partial_\theta\tau$ and $\partial_\theta^2\tau$,

$$\tau_0' = -\frac{2n\pi\sin\theta_0}{\nu - 2n\pi\varepsilon} = \frac{2n\pi\sqrt{1-(\nu - n\pi\varepsilon^2)}}{\nu - 2n\pi\varepsilon}, \tag{5}$$

$$\tau_0'' = \frac{2n\pi}{(\nu - 2n\pi\varepsilon)^3}\left[2n\pi\left(\varepsilon - \sqrt{1-(\nu - n\pi\varepsilon)^2}^{\,3}\right) - (\nu - n\pi\varepsilon)\left(\nu^2 - 2n\pi\varepsilon\nu + 2n^2\pi^2\varepsilon^2\right)\right]. \tag{6}$$

Equation (4) can be simply written by a quadratic function as

$$\Delta_{k+1} = f(\Delta_k) = \Delta_k(b + a\Delta_k), \tag{7}$$

where $a = \tau_0''/2$ and $b = 1 + \tau_0'$. From a standard quadratic mapping analysis, the stability condition for the fixed point θ_0 can be set as $|b| < 1$. If the stability condition is satisfied, the electron phase will converge to the fixed point as iteration goes on, even though there exists some perturbation in its trajectory.

We also considered the energy spread of the secondary electrons. To do that, the mapping function was modified as follows:

$$\theta_{k+1} = \theta_k + \tau(\nu_k, \theta_k) - \tau(\nu_0, \theta_0), \tag{8}$$

where $\nu_k = \nu_0 + \delta\nu_k$. As we use the Taylor expansion on Eq. (8) up to the second order, we approximately obtain

$$\theta_{k+1} = \theta_k + \Delta_k\tau_0' + \delta\nu_k\partial_\nu\tau_0 + \frac{1}{2}\Delta_k^2\tau_0'' + \Delta_k\delta\nu_k\partial_\nu\tau_0' + \frac{1}{2}\delta\nu_k^2\partial_\nu^2, \tag{9}$$

where $\Delta_k = \theta_k - \theta_0$. For the convenience in analysis, we represent Eq. (9) as follows:

$$g(x) = x(\hat{b} + ax) + s, \tag{10}$$

where $\hat{b} = b + \delta\nu_k\partial_\nu\tau_0'$, $s = \delta\nu_k\partial_\nu\tau_0 + \delta\nu_k^2\partial_\nu^2\tau_0/2$, $a = \tau_0''/2$, $b = 1 + \tau_0'$, $g(x) = \Delta_{k+1}$, and $x = \Delta_k$. In our previous work, we studied the case where $\delta\nu_k$ is small compared to the peak value of ν_0. Equation (10) was numerically calculated, and calculation of mapping was verified by PIC simulation.

III. EFFECTIVE LONGITUDINAL ENERGY SPECTRUM

In this section, we study the characteristics of the electron bunches, when more realistic features of secondary emission are included. Here, the realistic features can be described by two properties, which were not counted in our previous works:[1,2] one is the much wider energy spectrum of the secondary electrons and the other is the non-zero emission angle. The energy spread effect is already included in the mapping theory via the "s"-term in Eq. (10). Previously, we studied a very narrow, square-shaped emission energy spectrum,[1] where $\Delta\nu/\nu < 0.05 - 0.15$. Here, we apply the same mapping theory to the case with a broader, Gaussian-like realistic energy spectrum with $\Delta\nu/\nu < 0.1 - 0.5$. Furthermore, to account for the emission angle effects of the secondary electrons by the one-dimensional mapping theory,

Downloaded 01 Aug 2013 to 114.70.7.203. This article is copyrighted as indicated in the abstract. Reuse of AIP content is subject to the terms at: http://pop.aip.org/about/rights_and_permissions

we derived the "effective" emission spectrum of longitudinal velocity, which was implemented to the energy spread term in the mapping theory. The iteration results of the mapping were compared with PIC simulations. We also studied the electron bunching from a copper plate, which has even a wider emission energy spectrum. For such a very wide energy spectrum, our mapping theory is not valid any more, since Eq. (10) has derived from the Taylor expansion for small Δ_k only. In that case, we performed just the PIC simulations to obtain the electron bunching size in the phase space and current profile.

For the realistic energy spectrum and emission angle of the secondary electrons, we used the analytic fitting formulae in the paper by Furman and Pivi.[14] In Ref. 14, the authors described the energy distribution of secondary electrons from the surface of material, for a given energy and incident angle of a primary electron; the emission energy distribution of true secondary electrons is determined by $f_n(E) = F_n E^{P_n - 1} e^{-E/\varepsilon_n}$, where F_n is a normalizing factor, which depends on fitting parameters of material P_n, ε_n. This is for the true secondary emission, which dominates the energy spectrum more than other secondary emission mechanisms such as backscatter or rediffusion.[14]

As is implied from our one dimensional analysis, distribution of ν_z (longitudinal velocity) is important in determining the trajectories of electrons and bunching. At this point, we use velocity distribution instead of energy. The emission angle follows the $\cos\theta$ distribution, and azimuthal angle is uniformly distributed in 0–2π (Ref. 14) as in Fig. 2. The parallel component of the velocity does not influence much the bunching as long as the transverse dimension of the system is large enough compared to the transverse deviation of electrons for one cycle (this point was verified by PIC simulations). To obtain v_z-distribution with emission angle spread considered, we start from

$$E = \frac{1}{2}\frac{eE_a^2}{m\omega}\frac{\nu_z^2}{\cos^2\theta}, \tag{11}$$

which is from $E[\mathrm{eV}] = \frac{1}{2e}mv^2[\mathrm{eV}]$, $v = \frac{eE_a}{m\omega}\nu$, and $v = \frac{v_z}{\cos\theta}$. Emission angle and energy variation of the probability distribution can be expressed by $dP(E,\theta) = A\, f_n(E)\ \cos\theta\ d\theta\ dE$, where $f_n(E) = F_n E^{P_n - 1} e^{-E/\varepsilon_n}$ and A is a normalizing constant. Then, from Eq. (11), we obtain

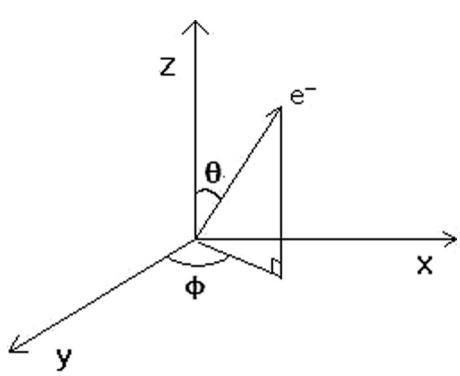

FIG. 2. The diagram of the θ distribution which follows $\cos\theta$ and ϕ is uniformly distributed in 0–2π.

$$dP(\nu_z,\theta) = \frac{A'\nu_z f_n'(\nu_z,\theta)}{\cos\theta}d\nu_z d\theta. \tag{12}$$

By averaging over ε, we obtain

$$dP(\nu_z) \approx \langle dP(\nu_z,\theta)\rangle_\theta d\nu_z = F(\nu_z)d\nu_z, \tag{13}$$

where $F(\nu_z) = \int_0^{\frac{\pi}{2}} \frac{A' f_n'(\nu_z,\theta)\nu_z}{\cos\theta}d\theta$. Here, $F(\nu_z)$ actually means the probability distribution of speed in z-direction considering the effect of the emission angle.

The numerical integration of $F(\nu_z)$ can be compared with velocity distribution obtained from Monte Carlo (MC) method. In MC method, we used the accept-reject method, where two random numbers are used. The procedures are that the first random number R_1 is chosen from the range $[0, E_{\max}]$, where $E_{\max}$ is the maximum true secondary electron energy. The first random number is used to calculate $f(R_1) = A'E^{P-1}e^{\frac{E}{\varepsilon}}$. Then, the second random number R_2 is uniformly generated between 0 and 1. The random number generation is repeated until we obtain $R_2 < f(R_1)$, then R_1 is converted to the normalized velocity $\nu = 2\omega\sqrt{R_1}/E_a$. We used 10^5 test electrons to get ν_z distribution. We compared the effective longitudinal velocity distributions calculated

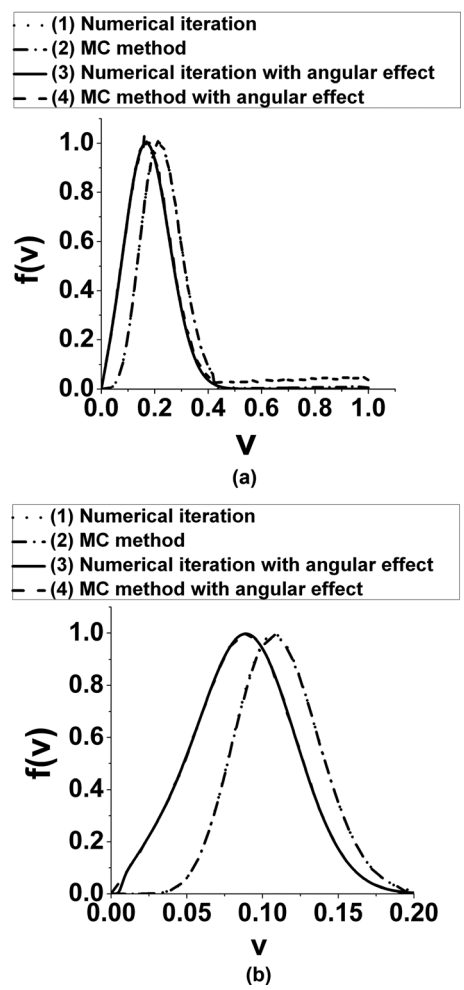

FIG. 3. Comparison of normalized velocity spectra between MC method and numerical iteration in artifical materials where the parameters are (a) $P_n = 64, \varepsilon_n = 0.01$ and (b) $P_n = 4.2, \varepsilon_n = 0.2$. The dotted and solid lines overlap quite exactly on the dotted-dashed and dashed lines, respectively, so they are not that distinguishable.

Downloaded 01 Aug 2013 to 114.70.7.203. This article is copyrighted as indicated in the abstract. Reuse of AIP content is subject to the terms at: http://pop.aip.org/about/rights_and_permissions

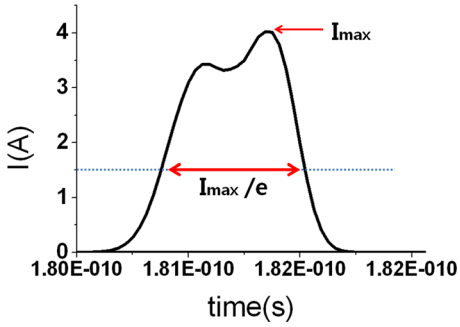

FIG. 4. (Color online) The current diagram of normal direction at the surface of material where the parameter of material is $P_n = 64, \varepsilon_n = 0.01$. We measured the full width of $I_{\max}/e$.

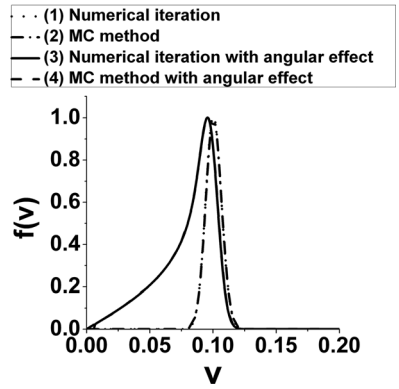

FIG. 6. Comparison of normalized velocity spectra between MC method and numerical iteration in copper case.

from Eq. (13) and from the MC calculation in Fig. 3. The material parameters were ($P_n = 65$, $\varepsilon_n = 0.01$) and ($P_n = 4.2$, $\varepsilon_n = 0.2$) which correspond to $\nu = 0.1 \pm 0.01$ and $\nu = 0.1 \pm 0.05$, respectively. These energy spreads are much wider than the cases in Ref. 1. From Fig. 3, it looks like that by the emission angle of secondary electrons, their effective longitudinal velocity distribution is generally broadened, and the peak position is shifted to the lower side. And in the case (a) of Fig. 3, which has narrower spectrum than Fig. 3(b), the peak position is shifted less; the shifted intervals of (a) and (b) are $\Delta\nu = 0.0044$ and 0.0186. On the other hand, the spectral width of ν_z in case (a) is much wider than case (b). Note that numerical iteration and MC method agree well with each other.

With these modified longitudinal velocity distributions of the secondary electrons, we iterated Eq. (10) to obtain phase diagrams. We also performed PIC simulations for comparisons. For the PIC simulations, the empirical formulae in Ref. 14 were implemented to the secondary electron routine of the code. The secondary emission routine allows a full energy spectrum of the secondary emission, which is composed of back scattering, rediffusion, and true secondary electron emission.[15] The width of material surface was 200 μm in transverse direction, and the longitudinal length of the system was 200 μm. We fixed the frequency and ac field amplitude at 35 GHz and 5.941 V/μm, respectively, and the dc field was varied.

To extract the phase information of the electron bunches from the PIC simulations, we measured the full width at $I_{\max}/e$ of the electric current through the emission plate as in Figure 4 and converted it to the phase following the procedure in Ref. 1. Electrons phase spread obtained in this way was compared with the results from mapping Eq. (10). Note that the width of the phase spread is proportional to the longitudinal size of the bunch. Figure 5 shows comparison of phase spread from the simulations and Eq. (10). The error bars actually represent the phase range measured from simulations. In this map, the shaded area means that the darker (blue online) the region is, the more frequently θ_k appear in that region during the interation of Eq. (10). In Fig. 5, the electrons phases mostly reside on the dark (blue online) region, whose ranges agree well with those measured from the simulations (full width $I_{\max}/e$). Figs. 5(a), 5(c) and 5(b), 5(d) are comparisons of the phase diagrams when the emission angle is counted [(b), (d)] or not counted [(a), (c)] for parameters corresponding to the cases of Fig. 3. In Figs. 5(a) and 5(c), both measured phases and calculated ones exhibit wider spread when the emission angle is counted, which is a natural result from the broadened effective ν_z-spectrum as

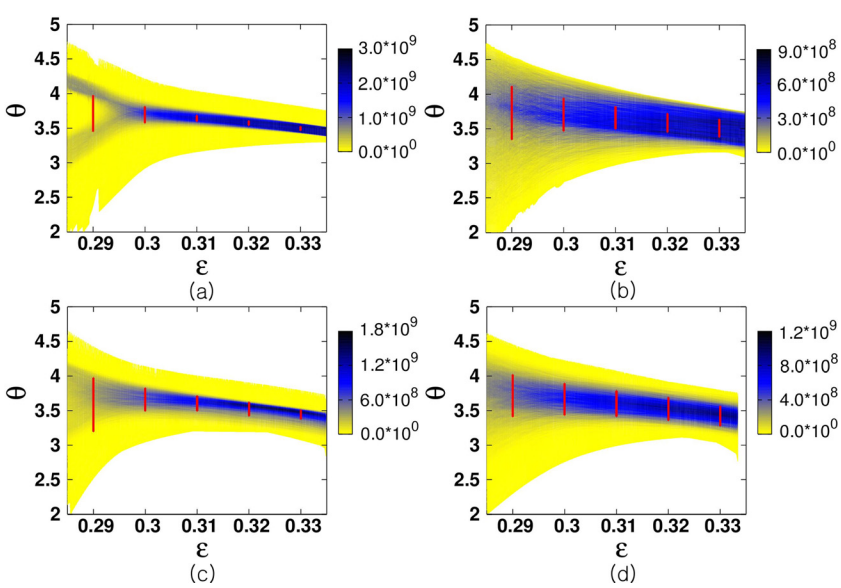

FIG. 5. (Color online) The diagram represented energy spread of secondary electron with angular effect, comparing with simulation results and mapping function, where the parameters are (a) $P_n = 64, \varepsilon_n = 0.01$ and (b) $P_n = 4.2, \varepsilon_n = 0.2$ without angular effect and (c) $P_n = 64, \varepsilon_n = 0.01$ and (d) $P_n = 4.2, \varepsilon_n = 0.2$ with effective angular effect.

Downloaded 01 Aug 2013 to 114.70.7.203. This article is copyrighted as indicated in the abstract. Reuse of AIP content is subject to the terms at: http://pop.aip.org/about/rights_and_permissions

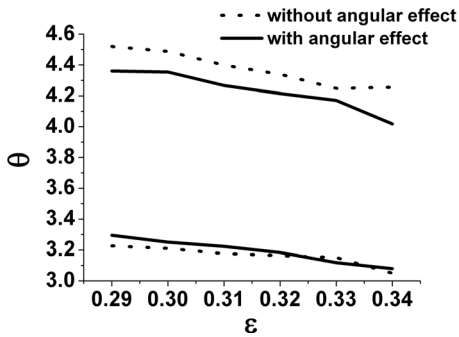

FIG. 7. PIC simulation of θ area of electron at the copper surface where ε is varied.

seen in Fig. 3(a). Note that the bifurcation [two branches of dark (blue online) region in Fig. 5(a)] is merged out in Fig. 5(c) by the broadened ν_z-spectrum by emission angle. In Figs. 5(b) and 5(d), the phase spread is a little bit wider when the angle effect is counted, which is opposite to the cases (a) and (c). This can be explained by different behavior of effective ν_z-spectrum in Figs. 3(a) and 3(b). In Fig. 3(b), the velocity broadening is not that significant as in Fig. 3(a), but instead, the peak shift to the lower side is severer. We observed from our previous work[1] that when the emission velocity is lower, the phase diagram shifts to the left in $\theta - \varepsilon$ space, which results in narrowing down of phase spread as shown in Fig. 5(d). In other words, depending on peak shift or spectral broadening of ν_z-distribution by emission angle, the phase spread (or correspondingly, the longitudinal bunch size) can be differently influenced.

Finally, we have considered the case of real parameters of P_n and ε_n for copper, which have much wider secondary energy spectrum as in Fig. 6. In this case, when the emission angle is counted, the peak shift appears quite significant ($\Delta\nu = 0.048$, corresponding to $2.28 \times 10^5 \mathrm{m/s}$), while the spectral broadening of ν_z-distribution is very small. So, we can expect, by the same logic discoursed for Figs. 5(b) and 5(d), the phase spread will be narrowed down. This point could be verified by the measurements from the PIC simulations. In Fig. 7, the upper (lower) curves represent the phase maximum (minimum) of electron trajectories as a function of $\varepsilon = E_d/E_a$. As the emission angle is counted (solid curves), the phase spread (distance from the lower curve to the upper curve) is narrowed down, which is similar to Figs. 5(b) and 5(d). The typical value of phase spread for copper is 4.747×10^{-12}s, corresponding to 80 μm in longitudinal bunch size.

IV. CONCLUSION

We studied the generation of beam bunching from dc-biased, single-surface multipactor with realistic energy spread and emission angle of secondary electrons. In our previous work, we theoretically studied stability condition of fixed phase and bifurcation, when the energy spectrum of the secondary electrons was quite narrow and the emission angle was neglected. In this paper, we extended our previous work to find the influences of much broader secondary emission spectrum and emission angle, which are always inherent in real materials. What we first considered here was the cases with somewhat artificial material with broad secondary energy spectrum and emission angle. The novel feature of this work is in employing the effective longitudinal velocity distribution to incorporate the emission angle effect to the one-dimensional quadratic mapping, which we used for theoretical analysis of the electron trajectories. We observed that when the emission angle is counted, the ν_z-distribution is effectively widened, and simultaneously there appears peak-shift to the lower side of ν_z. These two effects influence the phase spread (or the longitudinal bunch size), sometimes broadening it or sometimes narrowing it down, depending on which of spectral broadening or peak shift is dominant. We also studied the case where the copper, whose secondary spectrum is even wider, was used as an emission plate. In this case also, the bunch size slightly decreased by the emission angle effect: the numerical value of the longitudinal bunch size for copper was 80 μm, which is suitable for the generation of THz wave generation.

ACKNOWLEDGMENTS

This work was supported by KERI (Grant No. 11-12-N0101-27) and by ADD (Grant No. ADD-10-02-04-04).

[1]M. S. Hur, J.-Il. Kim, G.-Ju. Kim, and S. G. Jeon, Phys. Plasmas **18**, 033103 (2011).
[2]S. G. Jeon, J.-I. Kim, S.-T. Han, S.-S. Jung, and J. U. Kim, Phys. Plasmas **16**, 073101 (2009).
[3]E. F. Vance, J. Appl. Phys. **34**, 3237 (1963).
[4]H. C. Kim and J. P. Verboncoeur, Phys. Plasmas **12**, 123504 (2005).
[5]R. A. Kishek, Y. Y. Lau, L. K. Ang, A. Valfells, and R. M. Gilgenbach, Phys. Plasmas **5**, 2120 (1998).
[6]M. H. Greenblatt, Rev. Sci. Instrum. **20**, 646 (1949).
[7]S. Riyopoulos, Phys. Plasmas **14**, 112101 (2007).
[8]J. Rodney and M. Vaughan, IEEE Trans. Electron Devices **35**, 1172 (1988).
[9]R. Kishek and Y. Y. Lau, Phys. Rev. Lett. **75**, 1218 (1995).
[10]A. Frotanpour, G. Dadashzadeh, M. Shahabadi, and B. Gimeno, IEEE Trans. Electron Devices **58**, 876 (2011).
[11]C. Chang, G. Liu, C. Tang, C. Chen, and J. Fang, Phys. Plasmas **18**, 055702 (2011).
[12]L. Wu and L. K. Ang, Phys. Plasmas **14**, 013105 (2007).
[13]V. Semenov, V. Nechaev, E. Rakova, and N. Zharova, Phys. Plasmas **12**, 073508 (2005).
[14]M. A. Furman and M. T. F. Pivi, Phys. Rev. ST Accel. Beams **5**, 124404 (2002).
[15]G. Cheng and L. Liu, Comput. Phys. Commun. **182**, 1295 (2011).

Downloaded 01 Aug 2013 to 114.70.7.203. This article is copyrighted as indicated in the abstract. Reuse of AIP content is subject to the terms at: http://pop.aip.org/about/rights_and_permissions